water

MDPI

Article

Numerical Simulation of River Channel Change in the Suspended Sediment-Dominated Downstream Reach of the Sangu River

Md. Majadur Rahman †, Daisuke Harada * and Shinji Egashira

International Centre for Water Hazard and Risk Management (ICHARM), Public Works Research Institute (PWRI), 1-6, Minamihara, Tsukuba 305-8516, Ibaraki, Japan; majedst_buet@yahoo.com (M.M.R.); s-egashira77@pwri.go.jp (S.E.)

* Correspondence: d-harada55@pwri.go.jp; Tel.: +81-29-879-6779

† Current address: Bangladesh Water Development Board (BWDB), 72 Green Road, Pani Bhaban, Dhaka 1215, Bangladesh.

Abstract: This study aims to clarify the characteristics of the riverbed deformation, bank erosion, and channel changes in the lower Sangu River basin using a depth-averaged 2-D flow model where suspended sediment transport is dominant and its flow characteristics are influenced by active tides. A 45 km long area including the river mouth is computed using the 2-D model, and the results are compared with the observed channel changes. The computation results show that bed deformation and channel change are mainly caused during the ebb tide period of the spring tide particularly in an area of about 10 km from the river mouth. The detail study domain calculation results show that the flow concentration at the bend area causes the bed erosion there, and the eddy separated from the main stream causes the sediment deposition at the inner bank, while this eddy is not developed at the outer bank, resulting in the bank erosion there. Through these investigations, the characteristics and mechanisms of the morphodynamics in the lower Sangu River reach, particularly the potential of the combination of tides and floods to enhance riverbed deformations and the associated bank shifts, have been clarified.

Keywords: suspended sediment; river channel change; bank erosion; Sangu River

Citation: Rahman, M.M.; Harada, D.; Egashira, S. Numerical Simulation of River Channel Change in the Suspended Sediment-Dominated Downstream Reach of the Sangu River. *Water* **2024**, *16*, 1934. https://doi.org/10.3390/w16131934

Academic Editors: Bommanna Krishnappan, Tadaharu Ishikawa and Katsuhide Yokoyama

Received: 31 May 2024
Revised: 28 June 2024
Accepted: 7 July 2024
Published: 8 July 2024

1. Introduction

Bangladesh is located at the Bengal Delta, and it frequently experiences flood disasters due to the combination of heavy monsoon rains and the intense tidal fluctuations of the Bay of Bengal. During such floods, active channel change with bed deformation occurs, causing river channel changes, which in turn cause land loss in numerous locations.

The Sangu River is located in the southeastern part of Bangladesh, its catchment area is approximately 3600 km^2, and its downstream reach is lowland with significant meandering and tidal influence. The average bed slope of the lower Sangu River reach is 1/4700 and the representative sediment size is around 0.2 to 0.5 mm. In this area, the river channel has significant meanders, and active channel change occurs due to bank erosion, resulting in a large amount of land and houses lost every year and huge economic damages [1]. The channel change near the river mouth area is also affected by active tidal motions at the Bay of Bengal.

To prevent such damage, the river manager, Bangladesh Water Development Board (BWDB), has constructed bank protection works at several locations. However, as some of them have been damaged frequently, they need to repair the protection works from time to time [2]; thus, such countermeasures have not necessarily been efficient. To improve this situation, it is important to understand the characteristics and interactions between river flow, bed deformation, and associated bank erosion and channel migrations. Based on this

understanding, effective structural and non-structural countermeasures, such as suitable bank protection locations and evacuation and relocation plans, could be proposed.

Many studies have been conducted to investigate the processes of river meanders and their characteristics. Linear instability analysis is one way to understand the formation processes of sand bars and associated meanders [3–5]. These studies have shown that bar formation and its characteristics such as wave length and sinuosity are dominated by river regimes such as the width–depth ratio and the bed shear stress.

In field rivers such as the Sangu River, the meander migrates under the influence of the tides; thus, these bed deformations and meander migrations have nonlinear characteristics. Currently, such nonlinear characteristics are evaluated by numerical calculations. Struiksma et al. [6] and Shimizu and Itakura [7] proposed depth-averaged 2-D computation methods for the flow and bed deformation in meandering channels. In meandering channels, since bank erosion and channel change are closely related, methods to evaluate bank erosion have been proposed [8]. Nagata et al. [9] and Darby et al. [10] showed methods to compute bank erosion and channel changes in the depth-averaged 2-D computation fields. These methods are applied to simulate bank migration and channel changes in field rivers [11,12]. However, as many studies have pointed out, the erosion resistance of the riverbank depends on the conditions of each bank, such as the clay content of the soil and the vegetation [13,14]. Bank erosion resistance varies from place to place, making the general treatment of bank erosion difficult, and bank erosion resistance influences or dominates the characteristics of channel migration [15].

In addition to the complexity of the bank erosion and channel migration, the riverbed deformation in the Sangu River is mainly caused by suspended sediment transport [1]. In cases where the bed deformation is mainly caused by the bedload transport, the eroded sediment is deposited in relatively close areas where the bed shear stress is less than the critical shear stress, which causes channel change and sand bar migrations. On the other hand, in cases where the suspended sediment transport is dominant, sediment erosion occurs where the bed shear stress is relatively high, and the sediment deposition occurs uniformly at distant locations, especially with smaller particle sizes where the tendency is more apparent. Though several previous studies have attempted to simulate morphodynamics in suspended sediment dominated rivers [16–18], it is difficult to conclude that the entire processes or relationships between the suspended sediment erosion, deposition, bed deformation, bank erosion, and channel migration have been clarified.

This study aims to understand the characteristics of the riverbed deformation, bank erosion, and channel changes in the lower Sangu River basin using a depth-averaged 2-D flow model where suspended sediment transport is dominant and its flow characteristics are influenced by active tides. The calculation area spans around 45 km which includes the Bay of Bengal, and the available observed data such as water levels, flow discharges, and bank erosion are limited. This study is a practical and challenging approach that aims to apply 2-D flow simulations to mitigate damages caused by bank erosion and channel changes in the context of limited data, discussing the applicability and limitations of these methods.

2. Study Sites

The Sangu River originates from the Arakan Hill in Bangladesh, flows northwards, and discharges into the Bay of Bengal. The total catchment area of the basin is 3600 km^2, with approximately 80% of the area within hilly terrain and about 20% along coastal plain land. A 45 km long area from the river mouth has been selected as the study reach, as shown in Figure 1. The annual average rainfall of the basin is approximately 2750 mm [2], with 80% of the rainfall occurring during the monsoon season from June to September. For instance, Figure 2 shows the flow discharge observed at the Bandarban station from 10 June to 9 July 2018. It includes two peak flow discharges of nearly 1500 m^3/s, with the first peak lasting longer than the second peak. Figure 3 shows the water level data for the Khal No. 18 location, which is approximately 15 km north of the Sangu River mouth, for the

same period as Figure 2. Although water level data for the Sangu River mouth would be preferable for this investigation, they are unavailable due to the lack of a water level gauge at that location. Therefore, the water level at the Khal No. 18 location is shown here. Tides in the Bay of Bengal are semi diurnal with a prominent diurnal effect, i.e., two nearly equal high tides and two nearly equal low tides per day. The two cycles have slightly different amplitudes. Neap tide and spring tide are asymmetric, which means the water level varies significantly from neap to spring tides. In the eastern part of the coastal area of Bangladesh, the tidal range is macro-tidal [19]. The tidal ranges vary between −1.50 m and 3.50 m around the river mouth [20].

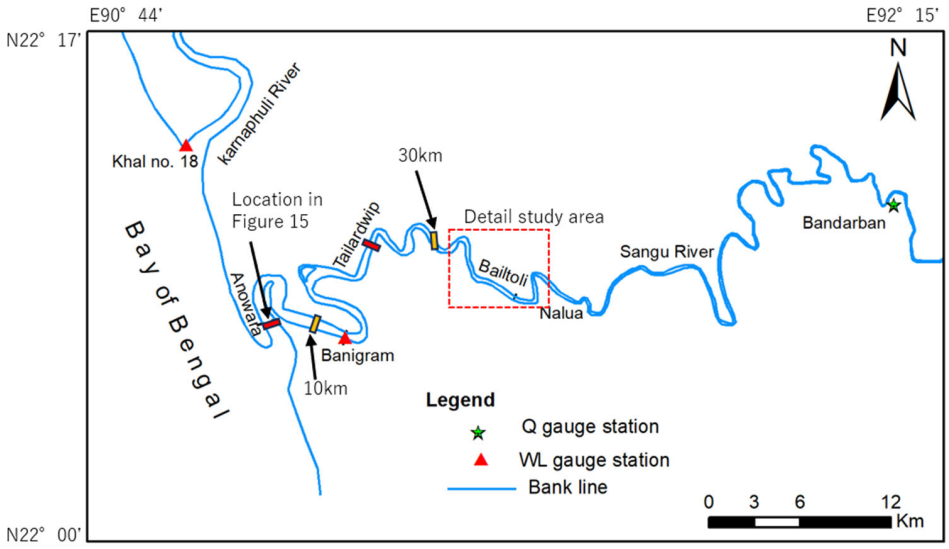

Figure 1. Study area (the lower Sangu River basin) and the location of gauge stations. The red dashed square shows the detail study area.

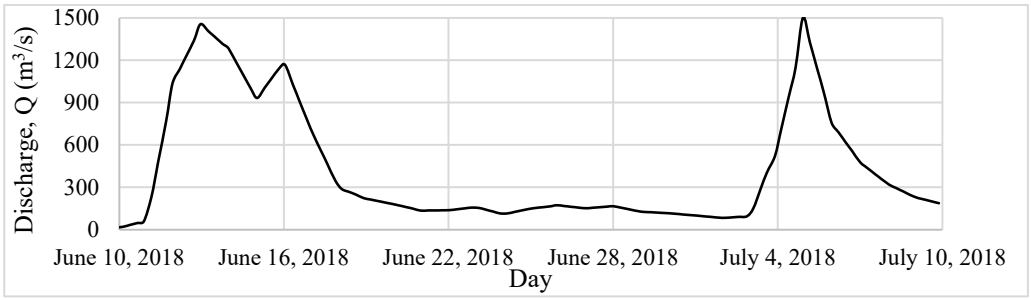

Figure 2. Flow discharge observed at Bandarban station from 10 June to 9 July 2018.

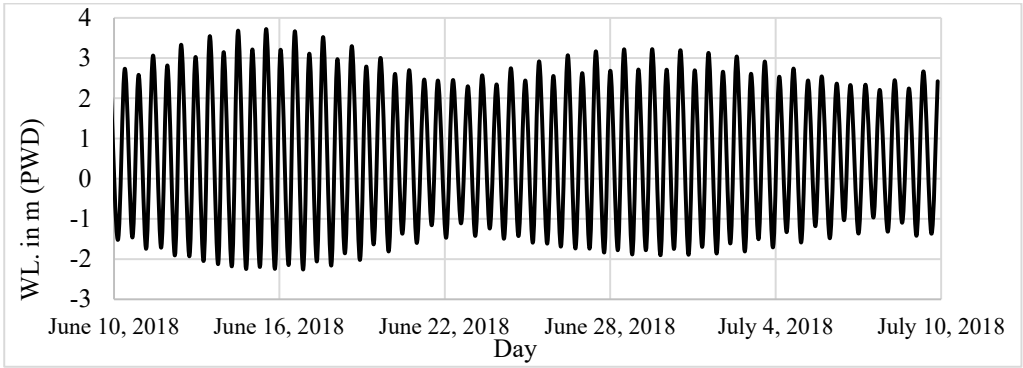

Figure 3. Observed water level at Khal No. 18 station [20]. The PWD is 0.46 m lower than the MSL.

According to Figure 3, the tidal variation during spring tide is approximately 5 m at the river mouth, suggesting strong mixing in the vicinity of the river mouth. Figure 4 shows the observed sediment size distribution. At the 10 km location, the representative sediment size is about 0.2 mm, indicating that buoyancy changes due to salinity do not significantly affect the settling velocity. Additionally, the ratio of river width to depth ranges from 50 to 100 in the study section, suggesting the possibility of predominant vertical mixing, which implies the applicability of the shallow water equations for the flow computation. Therefore, it is inferred that the bed sediment erosion rate model based on the concept of entrainment which was developed for the density stratified flows [21] is applicable for this study site. This concept allows direct sediment entrainment from the bed to the water, compared to conventional methods based on diffusion concepts at the reference level [22,23].

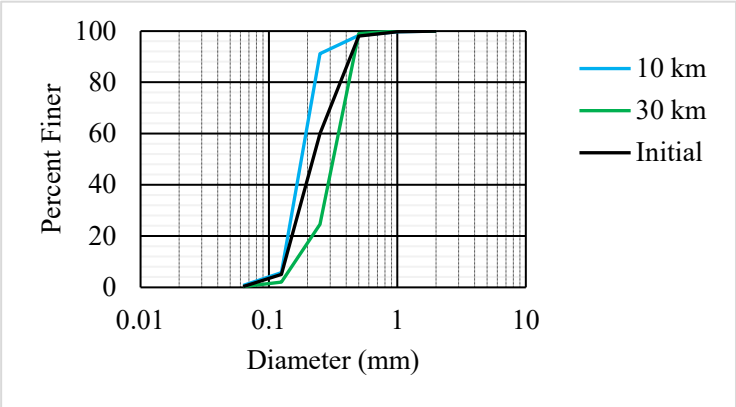

Figure 4. Observed sediment size distribution and initial sediment size distribution for the computation. Locations of 10 km and 30 km are shown in Figure 1.

3. Methodology

3.1. Flow Calculation with Bed Deformations

As discussed in the previous sections, the available observed data are limited within the very large study area, thus restricting the methodologies that can be applied to the target basin. Therefore, this study employs the two-dimensional shallow water equations to simulate the flow with fine sediment transport, using simple and feasible methods to understand the overall characteristics of the study sites.

The two-dimensional depth-averaged model with the momentum and continuity equations (iRIC-Nays2DH [24]) is used in this study. The computation framework of the depth-averaged two-dimensional governing equations of mass and momentum conservation equations for water flow are as follows:

$$\frac{\partial h}{\partial t} + \frac{\partial}{\partial x}(uh) + \frac{\partial}{\partial y}(vh) = 0 \tag{1}$$

$$\frac{\partial uh}{\partial t} + \frac{\partial uuh}{\partial x} + \frac{\partial uvh}{\partial y} = b_x - \frac{1}{\rho}\frac{\partial P}{\partial x} - \frac{\tau_{bx}}{\rho} + \frac{1}{\rho}\left(\frac{\partial h\tau_{xx}}{\partial x} + \frac{\partial h\tau_{yx}}{\partial y}\right) \tag{2}$$

$$\frac{\partial vh}{\partial t} + \frac{\partial uvh}{\partial x} + \frac{\partial vvh}{\partial y} = b_y - \frac{1}{\rho}\frac{\partial P}{\partial y} - \frac{\tau_{by}}{\rho} + \frac{1}{\rho}\left(\frac{\partial h\tau_{xy}}{\partial x} + \frac{\partial h\tau_{yy}}{\partial y}\right) \tag{3}$$

where h is the flow depth, t is the time, u, v, and b_x, b_y are the depth-averaged flow velocity and body force for the x and y directions, respectively, P denotes the total pressure, τ_{bx}, τ_{by} are the x and y components of bed shear stress, and ρ is the mass density of the water.

The suspended sediment transportation is evaluated within a depth-averaged 2-D flow field on the advection–diffusion equation as follows:

$$\frac{\partial c_i h}{\partial t} + \frac{\partial u c_i h}{\partial x} + \frac{\partial v c_i h}{\partial y} = \frac{\partial}{\partial x}\left(h\varepsilon_x \frac{\partial c_i}{\partial x}\right) + \frac{\partial}{\partial y}\left(h\varepsilon_y \frac{\partial c_i}{\partial y}\right) + E_i - D_i \tag{4}$$

where c_i is the depth-averaged suspended sediment concentration for the sediment size class i, ε_x and ε_y are the x and y components of the dispersion coefficient, respectively, and E_i and D_i are the erosion and deposition rates of the suspended sediment for the sediment size class i, respectively.

The erosion rate of the suspended sediment is evaluated using the entrainment velocity concept proposed by Harada et al. [21]:

$$E_i = p_i W_e \overline{c_s} \tag{5}$$

$$\frac{W_e}{U} = \frac{K}{R_{i*}} \tag{6a}$$

$$R_{i*} = (\sigma/\rho - 1)\overline{c_s} g h / \sqrt{u^2 + v^2}^2 \tag{6b}$$

where W_e is the entrainment velocity at the boundary between the upper water layer and the bedload layer, $\overline{c_s}$ is the sediment concentration on the bedload layer, R_{i*} is the overall Richardson number, and $K = 1.5 \times 10^{-3}$ [25]. In this study, we employ $\overline{c_s} = 0.2$ and the gravity force $g = 9.8\ (\mathrm{m/s^2})$.

The deposition rate is evaluated as follows:

$$D_i = w_{oi} c_i \tag{7}$$

where w_{oi} is the fall velocity of sediment particle size class i.

The riverbed deformation $\partial z_b / \partial t$ is evaluated as follows:

$$\frac{\partial z_b}{\partial t} + \frac{1}{1-\lambda}\sum_i \left(\frac{\partial q_{bix}}{\partial x} + \frac{\partial q_{biy}}{\partial y} + E_i - D_i\right) = 0 \tag{8}$$

where z_b is the bed elevation, λ is the porosity, q_{bix} and q_{biy} are the x and y components of the bedload transport rate for the sediment size class i, which is evaluated by the formula proposed by Egashira et al. (1997) [26] in this study.

3.2. Bank Shift in the 2-D Depth-Averaged Framework

As mentioned in the previous sections, bank erosion is a fundamental issue for river channel management in this region; thus, understanding its characteristics is crucial. Bank erosion is mainly caused as the block collapse of sediment in the vicinity of the riverbank. In case the riverbank does not contain much cohesive material, these collapses occur when the transverse riverbank slope exceeds the angle of repose. For example, Hasegawa [27] modeled such bank erosion processes in relation to the transverse bedload transport. Evangelista et al. [28] formulated a two-dimensional two-phase morphodynamic model accounting for geo-failure mechanisms over an unstructured triangular mesh. Asahi et al. [29] modeled bank erosion within a 2-D depth-averaged flow model framework by shifting whole grid systems as the bank shift proceeds. Though such treatment allows smooth bank shifts, the mass conservation of sediment is not kept when entire grid systems are modified in time. In addition, in case the grid size is large to compute a large area, there might be a gap between the scale at which the riverbank collapses in blocks and the scale of the computation grid. Biswas et al. [30] proposed a method to evaluate the bank erosion in response to riverbed erosion and deposition in the riverbank mesh, assuming that the bank shape keeps a similarity in time. This study employs this method within a 2-D depth-averaged flow model.

Figure 5 shows a schematic image of this method. The similarity approach assumes that in case the erosion of the riverbed ($\partial z_b/\partial t < 0$) is evaluated by Equation (5) in the bank grid, the unstable sediments that are eroded by the riverbed collapse and are deposited on the riverbed. Conversely, in case the sediment deposition ($\partial z_b/\partial t > 0$) is evaluated in the bank grid, the bank is developed.

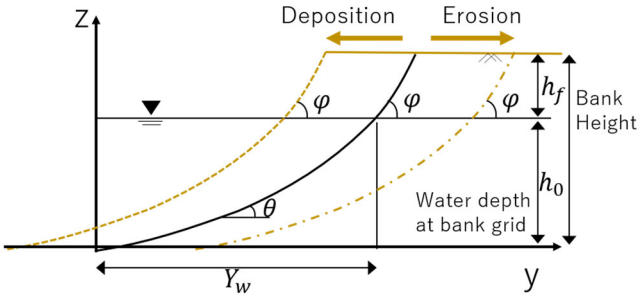

Figure 5. Schematic image of the bank shift. The figure made by Biswas et al. [30] is partially modified by the authors.

As shown in Figure 6, when the bank is shifted, the bank grid itself is moved in the transverse direction and the grids adjacent to the bank grid are stretched correspondingly. If the bank grid is close to an adjacent grid as a result of the bank shift, all quantities and variables in the bank grid are transferred to the adjacent grid, and the adjacent grid is defined as the new bank grid. This method allows us to treat bank shift in a 2-D depth-averaged model without compromising the mass conservation in the computational domain. To prevent computational instability, further bank movement is not calculated if the difference in bank position between the upstream and downstream grids is greater than 2Δy.

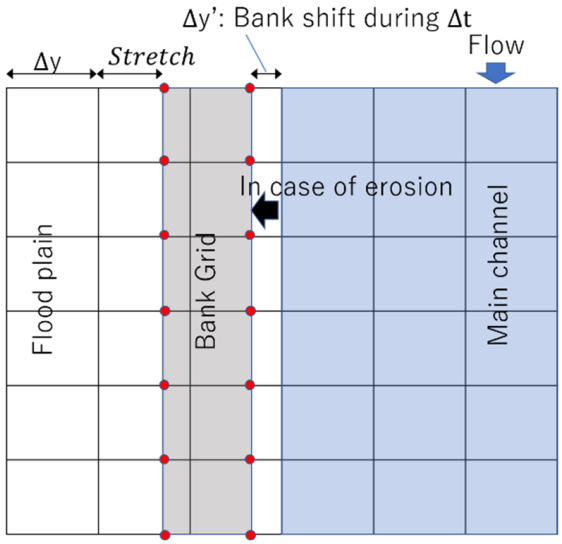

Figure 6. Conceptual diagram of grid movement due to the bank shift. The figure made by Biswas et al. [30] is partially modified by the authors.

4. Calculation Conditions

For the calculation domain, a large area covering the entire 45 km long lower Sangu River basin is prepared to understand the effect of tides on the morphodynamics. In addition, a small computation domain for the detailed study area, shown in Figure 1, is prepared to investigate characteristics of riverbed deformations with bank shift in the meandering area.

Bathymetry data surveyed in 2018 are used for the initial bed topography. For the large domain calculation, the 30-day flow discharge shown in Figure 2 is used as the upstream boundary condition. The downstream boundary water level is given with reference to Figure 3, so that the calculated water level and the observed water level at Banigram station coincide, which will be mentioned in the latter sections. The domain is extended from the river mouth to 15 km to the seaward and upstream boundary (45 km point) to 12 km upstream. The average cell size for the large area domain in the river area is approximately 30 m × 50 m.

For the detail study domain, the upstream end flow discharge and the downstream end water level are obtained from the large domain calculation results, and those are used as boundary conditions for the upstream discharge and the downstream water level, as shown in Figure 7. As for the computation duration, the discharge hydrograph shown in Figure 7 is repeated two times to investigate the characteristics of the bed deformation and associated channel change. The cell size for the detail domain is approximately 10 m square.

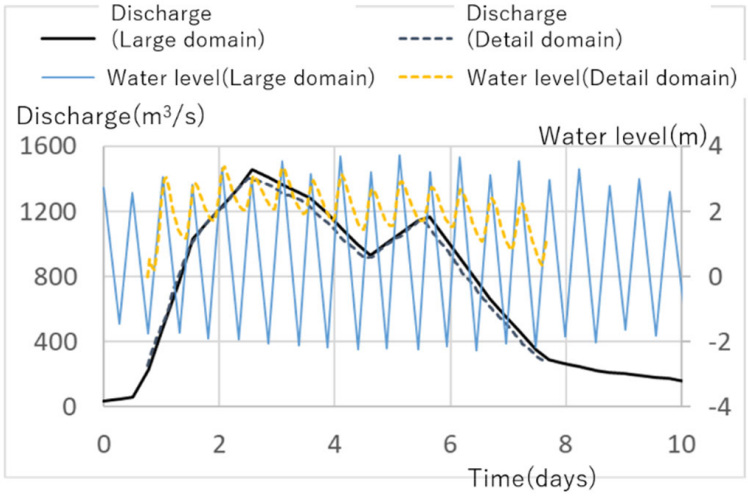

Figure 7. Boundary conditions for the large domain and small domain for the discharge and the water level.

Initial sediment size distributions for the both domains are set as shown in the black line of Figure 4 referring to the measured sediment size at 10 km and 30 km from the river mouth. The sediment size distribution in Figure 4 was divided into nine size classes, and the initial conditions were set according to the proportion of each grain size class. Manning's roughness coefficient is set as 0.03 for the both domains.

5. Results

5.1. Computation Validation

Figure 8 compares the simulated and observed water level at Banigram station from 13 June to 18 June for the spring tide, and Figure 9 also compares them for the neap tide from 20 June to 25 June. Though the observed data have some spikes (measurements are taken manually during the daytime; from 6:00 a.m. to 6:00 p.m.), it clearly shows the tidal fluctuation, and the simulated water level shows good agreement with the observed data.

As for the flow velocities, though no data are available for the calculation period, i.e., from 10 June to 10 July 2018, flow velocities were observed using ADCP on 9 October 2019 at Tailardwip station, thus the data are compared with the 2 July 2018 calculation results. Although the dates are different, the comparison is done here because the conditions of the two dates are similar in terms of the very low fresh water discharge and spring tides. The ADCP measurement was conducted at the Tailardwip station, and the depth-averaged velocity is compared with the observed velocity, as shown in Figure 10. Suspended sediment

concentration was measured at Bailtoli (see Figure 1) in 2020. The measurement was carried out from a boat, and discharge was measured by ADCP. At the same time, water samples were collected for measuring suspended sediment concentration. Several water samples were collected from various depths, and 21 surveys were conducted within three days. Figure 11 compares the measured suspended sediment discharge (Qs) with the all calculation results at the same location. Although it should be noted that this is not a direct comparison due to the different time periods, the two sets of data are generally consistent, especially when the flow discharge are high.

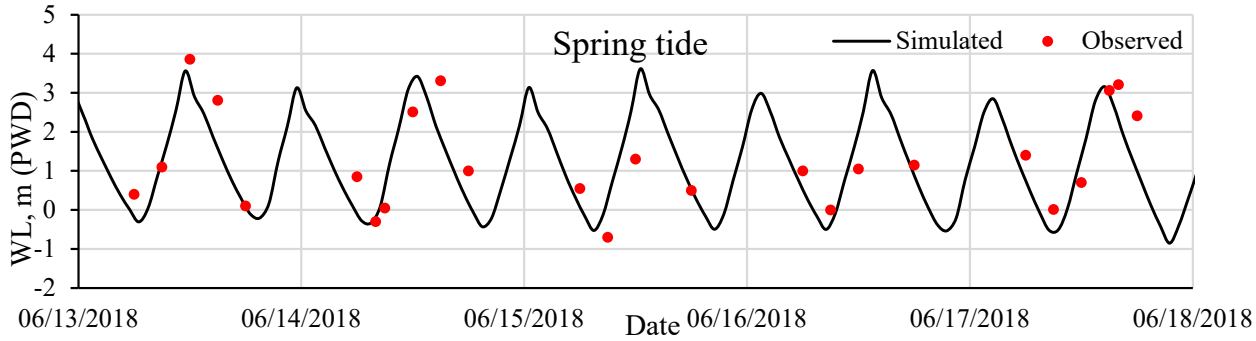

Figure 8. Comparison of simulated and measured water level at Banigram for spring tide (from 13 June to 18 June).

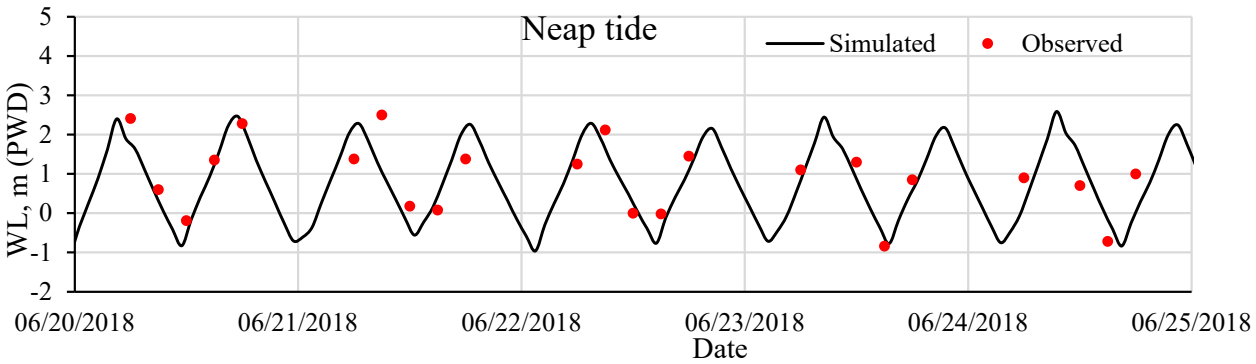

Figure 9. Comparison of simulated and measured water level at Banigram for neap tide (from 20 June to 25 June).

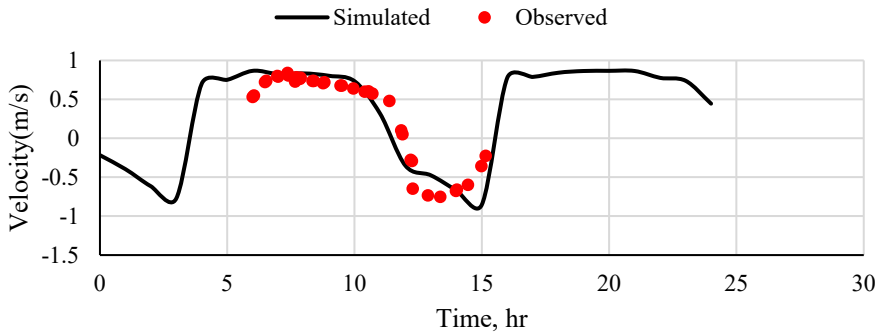

Figure 10. Comparison of the simulated flow velocity at the Tailardwip on 2 June with the observed flow velocity.

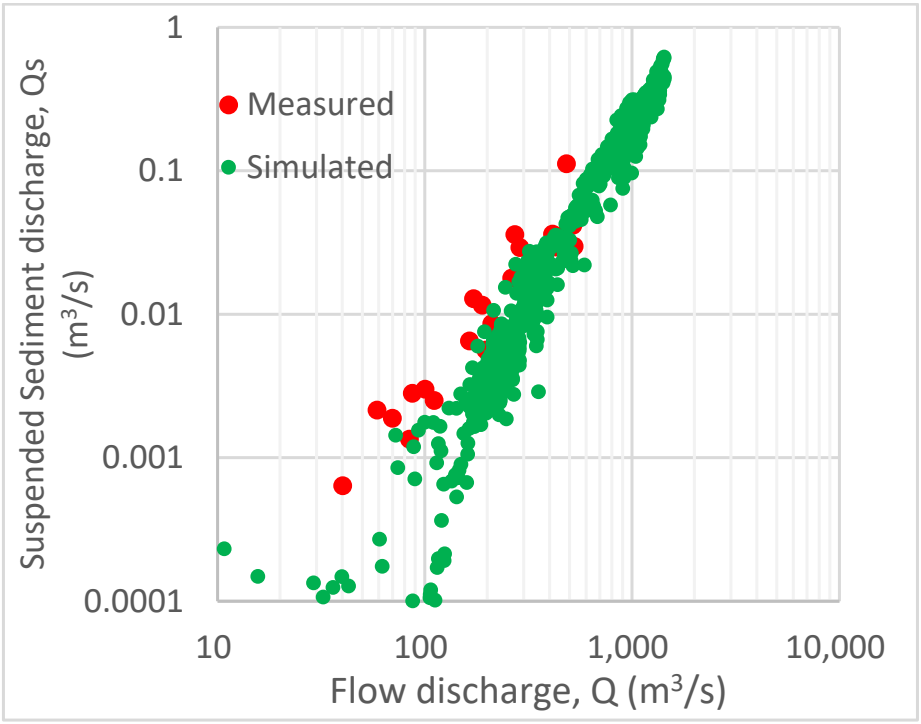

Figure 11. Comparison of the observed suspended sediment discharge.

5.2. Flow Characteristics for the Entire Domain

Figure 12a,b show the computation results at the peak discharge, during the high tide period and the low tide period, respectively. Computation durations and boundary conditions are shown in Figures 8 and 9. Figure 12c shows the spatial distribution of elevation change at the end of the computation period. During the high-tide period, the area circled in red in the figure is where the tidal flow and river flow intersect, and the riverbed deformation at this location is considerably smaller than those upstream and downstream. Upstream of this point, the river flow causes the riverbed deformation, while downstream of this point, the riverbed deformation is caused by the tidal flow and the river flow at low tide. Therefore, while the water level at the upstream side of the red circle in the figure is influenced by downstream tidal fluctuations, the flow causing bed deformation is mainly driven by river floods, which implies the applicability of the two-dimensional model for flow computation in the detailed study domain. It should be noted that the flow and associated riverbed deformation downstream of the red circle may be influenced by the saltwater wedge, which is not reproduced in the two-dimensional model. The next section discusses the results of riverbed deformations and bank shift conducted for this area.

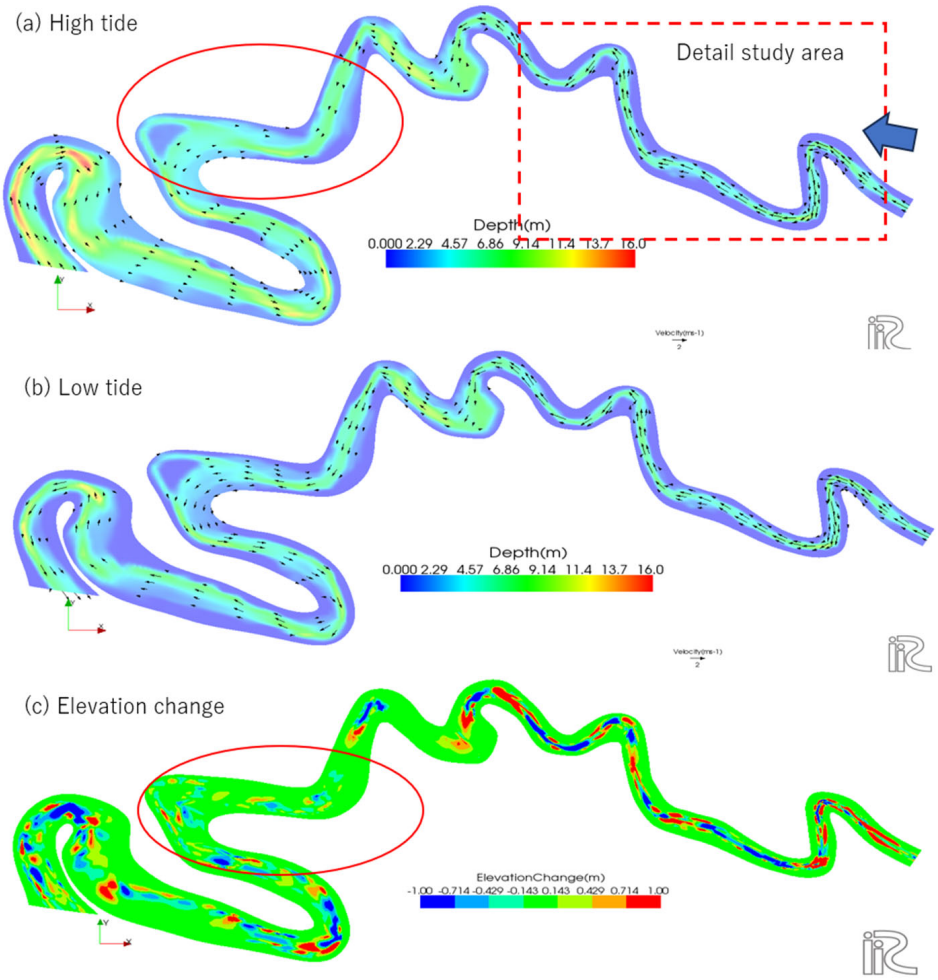

Figure 12. (**a**) Computation flow depth with velocity allow for the peak discharge during high tide. (**b**) Computation flow depth with velocity arrows for the peak discharge during low tide. (**c**) Bed elevation change at the end of the computation.

6. Discussions

6.1. Characteristics of Bed Deformation and Bank Shift

Topography measurements of the Sangu River were conducted in 2018 and 2020, and Figure 13a shows the bank shift and Figure 13b shows the bed deformation during this period. These figures show that riverbed deformations are active on the order of several meters, and that riverbank shift is also active. Comparison of the two figures shows that riverbank erosion occurs where the riverbed is eroding, e.g., (A), (B), and (C) shown in the figure. The trend is that riverbank erosions are observed on the outer banks downstream of the bend, e.g., (A), (C), and also on the inner banks of the bend such as (B) in Figure 13.

In order to compare Figure 13 with the computation results, although the computations should be performed for all of the four floods that occurred between 2018 and 2020, this is difficult because there were periods with missing observation data. Therefore, in this study, the 7-day flood shown in Figure 7 is repeated twice for a total of 14 days as a boundary condition, and the computation results are compared with the actual bed deformations shown in Figure 13b. Therefore, although the computation results are not directly compared with the measured data, the reproducibility of the channel change trend can be discussed.

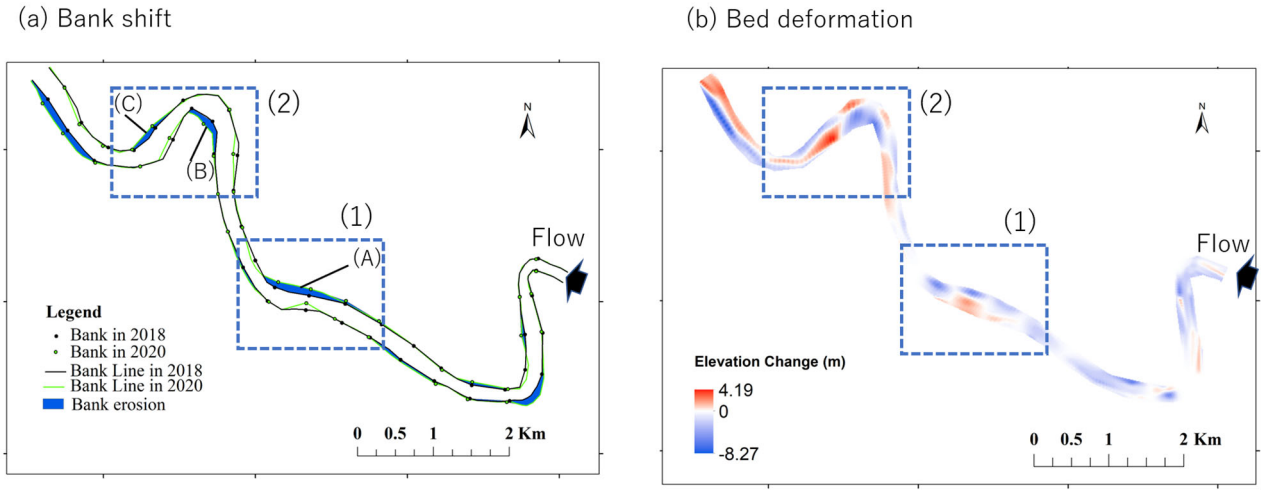

Figure 13. (**a**) Bank migration in 2018 and 2020, and (**b**) bed deformation in 2018 and 2020.

Figure 14 shows the computation results for area (1) including (A) and (2) including (B) and (C) in terms of bank shifts. In location (A), the right bank erosion and the sediment deposition along the left bank are reproduced. In location (C), the right bank erosion is reproduced. However, for the inner bank erosion in location (B), the bank erosion is not well reproduced. Indeed, it is possible that the erosion is caused by the stream line on the inner bank side of the bend, and such flow may be formed in the computation if a higher discharge is given as an upstream boundary condition, or it may not be possible to evaluate this inner bank flow without considering three-dimensional flow.

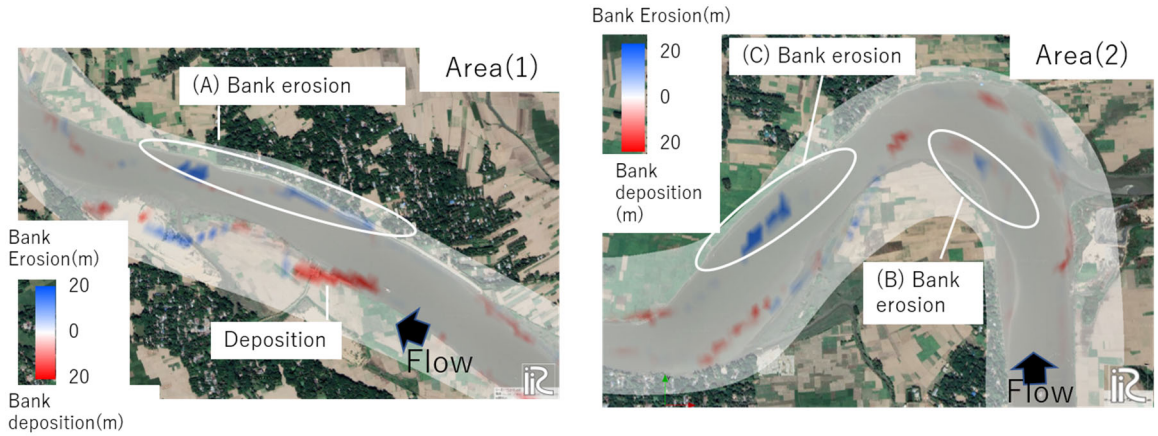

Figure 14. Bank migration in area (1) (**left**), and bank migration in area (2) (**right**).

6.2. Characteristics of Sediment Transport and Channel Change in the Tide-Dominated Area

Figure 12 shows that the morphological changes downstream of the red-circled area are caused by both tidal and flood currents. To investigate which of the tides and flow discharges causes the bed deformation and channel changes, calculations with different combinations of tidal amplitudes and flow discharge are conducted. The flow discharge is varied between 2000 (m^3/s) and 0 (m^3/s), and the tidal water level difference at the downstream end is varied between 2.5 m, 4.0 m, and 6.0 m. A level of 2.5 m corresponds to a neap tide and 6.0 m to a spring tide. Fifteen cases of combination are prepared, and flow and bed deformation computations are conducted for 10 days in each case. The computation results are shown in Figure 15 for the average volume of water and sediment passing through the Anowara location (shown in Figure 3 or near the downstream end of Figure 12). The results are shown separately for the ebb and high tides, which are defined by the direction of the flow velocity.

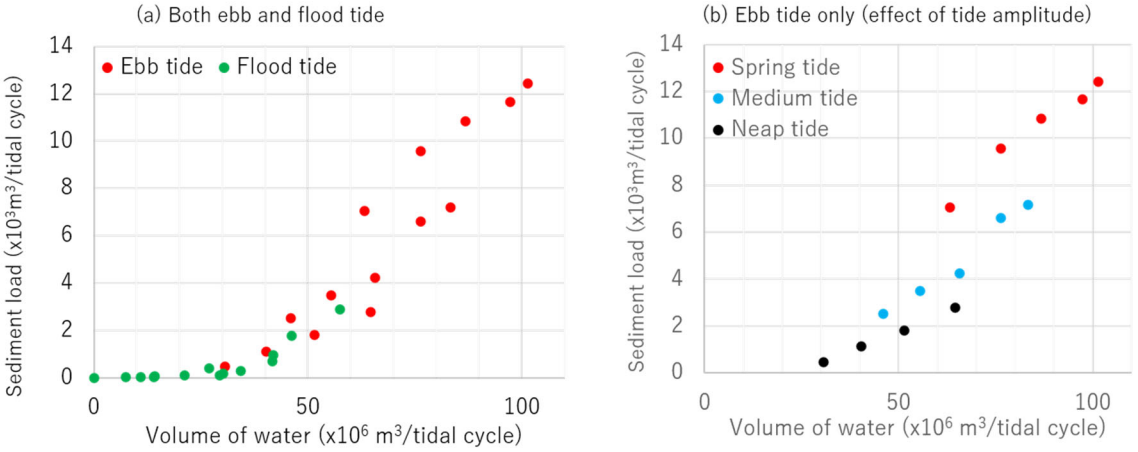

Figure 15. Computation results of 15 cases with different combinations of flow discharge and tide amplitudes at Anowara sites; (**a**) both results with ebb and flood tides, (**b**) ebb tides only with different tide amplitudes.

Figure 15 shows that both the amount of water and sediment passing through the Anowara section is small at high tide. When the amount of water passing through the section exceeds 40 ($\times 10^6$ m^3), the amount of sediment begins to increase. According to Figure 15b, the amount of sediment passing through the section is the largest during the spring tide. Thus, it is found that the bed deformation and topography change are active during the ebb tide period of the spring tide, even if the river discharge is relatively small. Since the spring tide occurs much more frequently compared to the river flood, it is estimated that the bed deformation in the downstream area of the red-circled area in Figure 12 is much more active compared to the upstream area where the bed deformation occurs only during the river flood, since the magnitudes of upstream and downstream bed deformation are similar in the computations for only 30 days with the two floods.

6.3. The Cause of Bank Migration and Channel Change Estimated by the Computation Results

This section discusses the cause of bank migration and channel change by comparing the computation results with the observed channel change. Figure 16 shows the spatial distribution of friction velocity at the first peak flow overlaid with the velocity vectors. In area (1), there are areas of high friction velocity in the near-straight channel where the flow is concentrated due to the formation of sandbars. In area (2), there are areas where the friction velocity is remarkably high along meanders with the curvature. Since the settling velocity of the sediment (about 0.3 mm in representative diameter) is about 0.05 (m/s), active suspended sediment transport occurs where the friction velocity is high. The distribution of velocity vectors in Figure 16 shows that in area (1), the main flow line curves toward the left bank, and an eddy detached from the main flow line is formed on the left bank side, i.e., the opposite bank of (A), and sediment is deposited at around this eddy because the friction velocity is small at the center of the eddy. As a result, bank deposition occurs on the left bank of the river, as shown in the measured data (right figure in Figure 13) and the computation results (left figure in Figure 14). On the other hand, in the area on the right bank side (A), a part of the flow overflows and inundation occurs, and the friction velocity is high where the inundated flow returns to the river channel. This flow erodes the riverbed in the vicinity of the riverbank, resulting in riverbank erosion in the right bank (A).

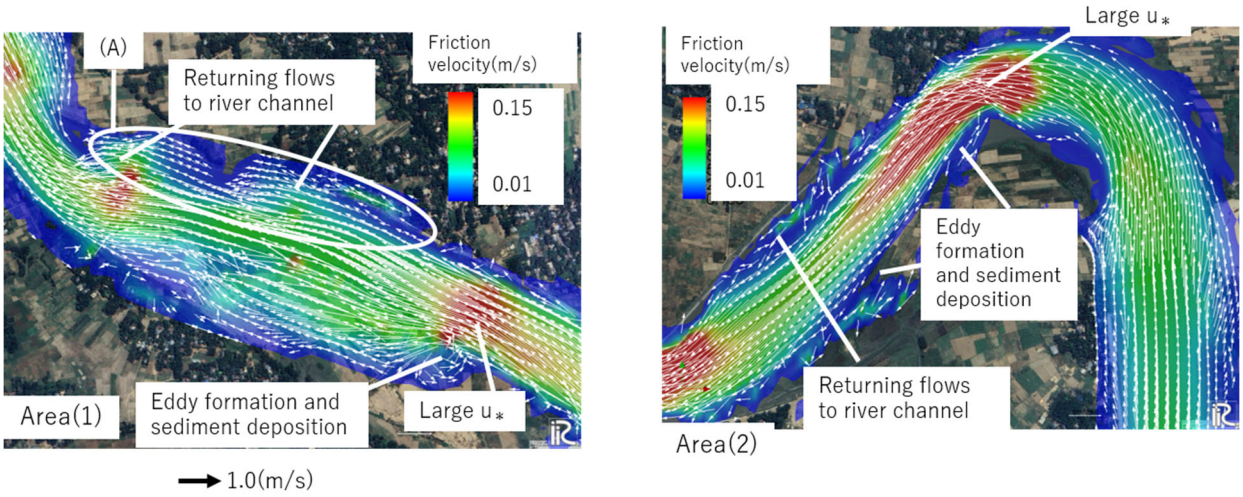

Figure 16. Friction velocity (u_*) distribution at the peak discharge with velocity distribution in area (1) (**left**) and in area (2) (**right**).

Similarly in area (2), a detached eddy is formed on the left bank side, i.e., the opposite bank of (C), and sediment is deposited at the center of the eddy where the friction velocity is small, as shown in Figure 17. On the other hand, in area c) on the right bank side, such eddies are partially formed, but these are not developed. Rather, when the overflowed water returns to the river channel, there is a place where the friction velocity is rather high, and riverbank erosion occurs at locations such as the outer bank side, as shown by the measurement (left figure in Figure 13) and the computation results (right figure in Figure 14).

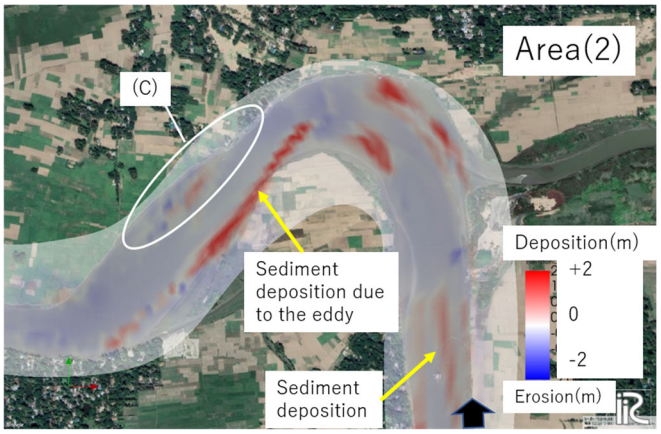

Figure 17. Bed elevation change at the end of the computation time in area (2).

Therefore, in the downstream of the bend, i.e., the flow concentration point, the entire meandering channel is gradually shifting downstream due to sediment deposition on the inner bank and riverbank erosion on the outer bank. Though it should be noted that these discussions are obtained by the 2-D flow computation under a certain condition, understanding the mechanism that the channel migration progresses in this way makes it possible to predict future channel changes and better channel planning and management.

7. Conclusions

In this study, a 2-D flow computation with bed deformation has been performed in the downstream reach of the Sangu River to understand the characteristics and mechanism of channel change and bank migration. We obtained the following findings and discussions through the comparison of the computation results with the field-observed data.

(1) The results of the large domain computations show that riverbed deformation is mainly caused by tides rather than river discharge in an area of about 10 km from the river mouth. In particular, a large amount of sediment is transported during the ebb tide period of the spring tide, resulting in active bed deformation and channel change in the downstream area.
(2) According to the computation results in the detailed study area, flood flows cause active bed deformation. In these areas, sediment deposition on the inner bank and bank erosion on the outer bank are observed just downstream of the bend.
(3) A detailed study area computation with bank shifts shows that on the inner bank downstream of the flow concentration area, suspended sediment is deposited along with the eddy separated from the main stream. This eddy is not developed on the outer bank side, and bank erosion at the outer bank is caused when the overflow water returns to the river channel. Therefore, the process of bank migration and channel change due to sediment deposition on the inner bank and erosion on the outer bank caused by suspended sediment transport is demonstrated. Such channel change is particularly accelerated during the ebb tide period of the spring tide.

Through these investigations, the characteristics and mechanisms of the morphodynamics in the lower Sangu River reach, particularly the potential of the combination of tides and floods to enhance riverbed deformations and the associated bank erosion and its migration, have been clarified.

Author Contributions: M.M.R., D.H. and S.E. designed the study. M.M.R. and D.H. performed the numerical simulations, and wrote the paper. S.E. reviewed and edited the paper. All authors have read and agreed to the published version of the manuscript.

Funding: This research was funded by the Japan Society for the Promotion of Science (grant no. 22K14334).

Data Availability Statement: The authors will declare the available data here after publication.

Acknowledgments: The authors would like to express their gratitude to the Bangladesh Water Development Board (BWDB) and JICA for their data collection and financial support for this study.

Conflicts of Interest: The authors declare no conflicts of interest.

References

1. Rahman, M.M.; Harada, D.; Egashira, S. Basin Scale Sediment Transport Processes Using Rainfall Sediment Runff Model—A Case Study of Sangu River Basin. *J. Jpn. Soc. Civ. Eng. Ser. B1 (Hydraul. Eng.)* **2022**, *78*, I_1099–I_1104. [CrossRef]
2. Bangladesh Water Development Board (BWDB), Institute of Water Modelling (IWM), Feasibility Study for Restoration of Sangu and Matamuhuri River Basin. 2021. Available online: http://www.kmcltd.org/smrb_project.php (accessed on 28 November 2023).
3. Ikeda, S.; Parker, G.; Sawai, K. Bend theory of river meanders. Part 1. Linear development. *J. Fluid Mech.* **1981**, *112*, 363–377. [CrossRef]
4. Blondeaux, P.; Seminara, G. A unified bar–bend theory of river meanders. *J. Fluid Mech.* **1985**, *157*, 449–470. [CrossRef]
5. Kuroki, M.; Kishi, T. Regime criteria on bars and braids in alluvial straight channels. *Proc. Jpn. Soc. Civ. Eng.* **1984**, *1984*, 87–96. [CrossRef] [PubMed]
6. Struiksma, N.; Olsen, K.W.; Flokstra, C.; De Vriend, H.J. Bed deformation in curved alluvial channels. *J. Hydraul. Res.* **1985**, *23*, 57–79. [CrossRef]
7. Shimizu, Y.; Itakura, T. Calculation of bed variation in alluvial channels. *J. Hydraul. Eng.* **1989**, *115*, 367–384. [CrossRef]
8. Osman, A.M.; Thorne, C.R. Riverbank stability analysis. I: Theory. *J. Hydraul. Eng.* **1988**, *114*, 134–150. [CrossRef]
9. Nagata, N.; Hosoda, T.; Muramoto, Y. Numerical analysis of river channel processes with bank erosion. *J. Hydraul. Eng.* **2000**, *126*, 243–252. [CrossRef]
10. Darby, S.E.; Alabyan, A.M.; Van de Wiel, M.J. Numerical simulation of bank erosion and channel migration in meandering rivers. *Water Resour. Res.* **2002**, *38*, 2–1–2–21. [CrossRef]
11. Bosa, S.; Petti, M.; Pascolo, S. Numerical modelling of cohesive bank migration. *Water* **2018**, *10*, 961. [CrossRef]
12. Iwasaki, T.; Shimizu, Y.; Kimura, I. Numerical simulation of bar and bank erosion in a vegetated floodplain: A case study in the Otofuke River. *Adv. Water Resour.* **2016**, *93*, 118–134. [CrossRef]
13. Micheli, E.R.; Kirchner, J.W. Effects of wet meadow riparian vegetation on streambank erosion. 1. Remote sensing measurements of streambank migration and erodibility. *Earth Surf. Process. Landf.* **2002**, *27*, 627–639. [CrossRef]

14. Collins, D.B.G.; Bras, R.L.; Tucker, G.E. Modeling the effects of vegetation-erosion coupling on landscape evolution. *J. Geophys. Res. Earth Surf.* **2004**, *109*, 1–11. [CrossRef]
15. Ahmed, T.S.; Egashira, S.; Harada, D.; Yorozuya, A. Sediment Transportation and Sand Bar Deformation Owing to Tidal Currents in Sittang River Estuary, Myanmar. *J. Jpn. Soc. Civ. Eng. Ser. B1 (Hydraul. Eng.)* **2019**, *75*, I_1027–I_1032. [CrossRef]
16. Duan, J.G.; Nanda, S.K. Two-dimensional depth-averaged model simulation of suspended sediment concentration distribution in a groyne field. *J. Hydrol.* **2006**, *327*, 426–437. [CrossRef]
17. Xie, Q.; Yang, J.; Lundström, T.S. Field Studies and 3D Modelling of Morphodynamics in a Meandering River Reach Dominated by Tides and Suspended Load. *Fluids* **2019**, *4*, 15. [CrossRef]
18. Masbahul, I.M.; Yorozuya, A.; Harada, D.; Egashira, S. A Numerical Study on Bank Erosion of a Braided Channel: Case Study of the "Tangail and Manikganj Districts Along the Brahmaputra River". *J. Disaster Res.* **2021**, *17*, 263–269. [CrossRef]
19. Bangladesh Inland Water Transport Authority (BIWTA), Government of People's Republic of Bangladesh Ministry of Shipping, Bangladesh Regional Waterway Transport Project 1. 2019. Available online: https://biwta.portal.gov.bd/sites/default/files/files/biwta.portal.gov.bd/page/f3ca1ff6_95b0_4606_849f_2c0844e455bc/Revised_Final%20Report%20(Main%20Report).pdf (accessed on 28 November 2023).
20. Uddin, M.; Alam, J.B.; Khan, Z.H.; Hasan, G.M.J.; Rahman, T. Two Dimensional Hydrodynamic Modelling of Northern Bay of Bengal Coastal Waters. *Comput. Water Energy Environ. Eng.* **2014**, *3*, 140–151. [CrossRef]
21. Harada, D.; Egashira, S.; Ahmed, T.S.; Ito, H. Entrainment of bed sediment composed of very fine material. *Earth Surf. Process. Landf.* **2022**, *47*, 3051–3061. [CrossRef]
22. van Rijn, L.C. Mathematical modeling of suspended sediment in nonuniform flows. *J. Hydraul. Eng.* **1986**, *112*, 433–455. [CrossRef]
23. Itakura, T.; Kishi, T. Open channel flow with suspended sediments. *J. Hydraul. Div.* **1980**, *106*, 1325–1343. [CrossRef]
24. Shimizu, Y.; Nelson, J.; Arnez Ferrel, K.; Asahi, K.; Giri, S.; Inoue, T.; Iwasaki, T.; Jang, C.L.; Kang, T.; Kimura, I.; et al. Advances in Computational Morphodynamics Using the International River Interface Cooperative (iRIC) Software. *Earth Surf. Process. Landf.* **2019**, *45*, 11–37. [CrossRef]
25. Egashira, S.; Ashida, K. Studies on the structures of density stratified flows. *Bull. Disaster Prev. Res. Inst. Kyoto Univ.* **1980**, *29*, 165–198.
26. Egashira, S.; Miyamoto, K.; Ito, T. Constitutive equations of debris flows and their applicabilities, Debris Flow Hazards Mitigation. In Proceedings of the First International Conference, Water Resources Engineering Division/ASCE, San Francisco, CA, USA, 7–9 August 1997; pp. 340–349. [CrossRef]
27. Hasegawa, K. Universal bank erosion coefficient for meandering rivers. *J. Hydraul. Eng.* **1989**, *115*, 744–765. [CrossRef]
28. Evangelista, S.; Greco, M.; Iervolino, M.; Leopardi, A.; Vacca, A. A new Algorithm for Bank-Failure Mechanisms in 2D Morphodynamic Models with Unstructured Grids. *International J. Sediment Res.* **2013**, *30*, 382–391. [CrossRef]
29. Asahi, K.; Shimizu, Y.; Nelson, J.; Parker, G. Numerical simulation of river meandering with self-evolving banks. *J. Geophys. Res. Earth Surf.* **2013**, *118*, 2208–2229. [CrossRef]
30. Biswas, R.K.; Yorozuya, A.; Egashira, S. Numerical Model for Bank Erosion in the Brahmaputra River. *J. Disaster Res.* **2016**, *11*, 1073–1081. [CrossRef]